Journal of Sound and Vibration (1999) **223**(3), 379–398
Article No. jsvi.1998.2132, available online at http://www.idealibrary.com on IDEAL®

THE CONVECTIVE AND ABSOLUTE INSTABILITY OF FLUID FLOW OVER VISCOELASTIC COMPLIANT LAYERS

K. S. Yeo, B. C. Khoo and H. Z. Zhao
Department of Mechanical and Production Engineering, National University of Singapore, Kent Ridge Crescent, 119260 *Republic of Singapore*

(*Received* 22 *December* 1997, *and in final form* 2 *December*, 1998)

The occurrence of waves on viscoelastic compliant layers subject to fluid flow is studied from the viewpoint of their classification as convective and absolute instability of the flow-wall system. Uniform potential flow and modified potential flows representing laminar and turbulent boundary layers are considered. It is found that uniform potential flow over viscoelastic (dissipative) layer admits only absolute instability, whereas convective and absolute instability modes may be found under laminar and turbulent boundary layers. The onset velocity of absolute instability remains nearly constant with changes in wall damping, with a value of about $3C_t$ for turbulent boundary layers, where C_t is the elastic shear wave speed of the compliant material. Convective instability always occurs at a lower flow velocity than absolute instability. The onset velocity for convective instability, on the other hand, increases fairly rapidly with wall damping and tends towards the onset velocity for absolute instability in the case of a highly damped layer. The results suggest that the static divergence waves observed on highly damped coatings in experiments are manifestation of absolute instability.

1. INTRODUCTION

The experiments of Gad-el-Hak *et al*. [1], Gad-el-Hak [2] and Hansen *et al*. [3] show that surface waves on viscoelastic compliant walls under a turbulent boundary layer may be divided into two categories: the slow waves and the fast waves. The slow waves, which have also been termed *static divergence waves*, are found on compliant layers possessing a significant level of material damping, whereas the fast waves, which have phase speeds in the range of 30–50% of the free-stream velocity had only been observed on nearly elastic layers. With the notable exceptions of Duncan *et al*. [4] and Evrensel and Kalnins [5], much of the theoretical studies of flow over compliant surfaces have tended, however, to focus on stability of flows in their laminar state. The motivation for the laminar work, such as those of Carpenter and Garrad [6] and Yeo [7] to name a few, has come mainly from a desire to understand the conditions under which compliant walls may delay the transition of laminar boundary layers to a turbulent state,

0022–460X/99/230379 + 20 $30.00/0

and thus realize the much sought-after benefit of drag reduction that comes with transition delay. However, turbulent flows are more prevalent in nature. Knowledge of their interaction with compliant layers is equally important since the occurrence of the slow waves, which generally have large-amplitudes, will increase skin-friction drag via their roughness action. Gad-el-Hak *et al.* [1] noted that the structures of turbulent boundary layers are also modified in the presence of the slow waves. These have implications for the use of compliant materials as acoustic coatings in underwater applications

The occurrence of surface waves on compliant or flexible walls subjected to flow, be it laminar or turbulent, can generally be viewed as arising from an instability of the flow-wall dynamical system in coupled interaction. Adopting this viewpoint, Benjamin [8] and Landahl [9] applied normal-mode temporal stability theory to the study of flow over flexible membrane surfaces. Normal-mode temporal stability theory assumes the instabilities to be sinusoidal waves of uniform amplitude in space that grow in time. They showed that the flow–flexible wall system can theoretically support a variety of instability waves in addition to derivatives of the well-known Tollmien–Schlichting (TS) waves that are found in an unstable laminar boundary layer over a rigid flat plate. The additional waves were clearly brought into being by the compliant quality of the wall, and were termed Flow-induced Surface Instability by Carpenter [6] and Compliance-induced Flow Instability by Yeo [7] to emphasize their different origin from the TS waves. They were shown to arise from the unstable dynamical interplay between the inertial quality of the flow and the *dynamic* and *static* deformation modes of the compliant wall. The former leads to waves that travel at a fair speed (termed *travelling wave flutter* or TWF for short) and the latter produces nearly static or slowly moving waves (termed *static divergence* or SD for short). Yeo and Dowling [10] were able to derive general criteria that relate the stability of these waves to the dynamic and static wave-bearing characteristics of a compliant wall. Benjamin [8] and Landahl [9] also showed that, despite these new instabilities being created, wall compliance is actually stabilizing on the TS waves. Furthermore, Landahl [9] and Benjamin [11] were able to clarify the important and sometimes anomalous effect of wall damping on the various instabilities by invoking energy arguments. Benjamin [11] assigned a classification of the instability waves based on a concept of the *activation* energy of a wave. The TWF modes have positive activation energy and are Class B in Benjamin's classification. Such a wave would be attentuated by energy loss from the dynamical system, such as would be caused by increased wall damping. The TS waves are Class A and have negative activation energy. They actually strive on increased wall damping, that causes energy loss from the system. The SD waves are frequently classified as a Class A because they are frequently destablized by increase in wall damping and appear to require wall damping for their occurrence. Benjamin also introduced a Class C wave. Class C wave phenomena are characterized by mainly conservative exchange of wave energy between the flow and the wall, and tend to be relatively insensitive to small variation in wall damping.

The surface waves in the turbulent-flow experiments of Gad-el-Hak *et al.* [1] and Gad-el-Hak [2] clearly represent deviations from mean-flow conditions that

could not be ascribed to turbulent fluctuations. In the context of temporal stability theory, the slow and fast waves clearly correspond in character to the TWF and the SD waves. Both Duncan *et al.* [4] and Evrensel and Kalnins [5] employed the *normal-mode temporal* theory of instability in their study of laminar and turbulent layers over viscoelastic compliant layers. Duncan *et al.* investigated theoretically the occurrence of slow-wave instability on viscoelastic layers by assuming the pressure fluctuations of the flow to be given by that of potential flow modified by a complex scaling factor of the form $K_t e^{i\theta_p}$. Values of K_p and θ_p were obtained from literature to simulate the perturbative actions of both laminar and turbulent boundary layers on the compliant surfaces. Despite the simplicity of the flow model, Duncan *et al.*'s results display a high degree of qualitative consistency with the experimental results of Gad-el-Hak *et al.* [1]. Evrensel and Kalnins [5] employed a more elaborate flow model (viscous) to study the onset of slow and fast waves. The turbulent boundary layers were represented by their mean-velocity profile. The contributions of turbulent stresses to the dynamics of perturbation were neglected however. They were able to obtain good quantitative agreement with the results by Gad-el-Hak *et al.* on the onset flow velocities and phase speeds of the instabilities, but not on wavelengths.

The normal-mode temporal theory models only the variation of a wave with respect to time. This representation of wave instability is satisfactory for a compact (closed) dynamical system. But it becomes inadequate when carried over to open dynamical systems, such as in flow past a flat plate, where the evolution of waves may display non-uniformity in space due to growth or decay in space directions. The popularity of the temporal theory in literature on hydrodynamic stability is due in no small degree to its relative simplicity. While the temporal theory will undoubtedly continue to play an important role for the local analysis of open systems, a more complete theoretical model of wave evolution in open systems is given by the time-asymptotic spatial-temporal theory of Briggs [12]. Briggs shows via a rigorous spatio-temporal analysis, which takes into account causal factors, that the instabilities in open physical systems tend to evolve in one of two physically distinct manners: an unstable disturbance may grow in size as it propagates away from its initiating source; or it may grow with time in an ever-expanding neighbourhood of the source. In the first case, the instability is said to be *convective*. At any fixed spatial position away from the source, the instability wave eventually vanishes when the initiating source is turned off. An instability growing by the second mode is termed an *absolute instability*. Once excited, an absolute instability is self-sustaining. At any fixed spatial position, the disturbance grows with time until its growth is ultimately delimited by non-linear dynamical factors. An absolute instability is clearly a much more devastating form of instability than a convective instability. Moreover, because the group velocity of an absolute instability wave mode is zero, it may assume a stationary or nearly stationary appearance at its onset.* A more recent account of the theory of convective and

* The concept of group velocity as the propagation velocity of wave energy is meaningful only for neutral and slightly unstable waves.

absolute instabilities is given by Bers [13]. The spatio-temporal model is by far a more complex model of wave evolution than the standard normal-mode model, both in theory and in implementation. It is only with the development in recent years of more effective algorithms that the spatio-temporal theory has now grown beyond applications to highly idealized stability problems in analytical form.

The experimental observations of the fast and slow waves by Gad-el-Hak *et al.* [1] and Gad-el-Hak [2] are more or less in accord with the theoretical dichotomy of convective and absolute instabilities as described above. The stability of flow over viscoelastic compliant layers is re-examined in this paper from the viewpoint of their classification as absolute and convective instabilities. For this study, the modified potential-flow approach of Duncan *et al.* [4] has been adopted in modelling the flow. The model is simple, but yet possesses sufficient flexibility for the perturbation responses of both laminar and turbulent boundary layers to be approximated within a single theoretical framework. It could be argued that the model is over-simplistic. However, the good consistency of its results with the experimental observations is proof of the model's adequacy in representing the cardinal physics of the flow (when the appropriate values of K_p and θ_p are used); and one could be reasonably confident that the model will yield correct qualitative stability behaviour even though the numerical values themselves may lack in accuracy.

The dispersion relation for wave stability is formulated as a generalized matrix eigenvalue problem following Yeo *et al.* [14], who have shown that absolute instability modes do in fact exist in a Blasius boundary layer over soft damped compliant layers. Results for absolute and convective instabilities in potential flow and laminar and turbulent boundary layers are obtained and their relations to the observed occurrences of slow and fast waves are discussed.

2. THE STABILITY EIGENVALUE PROBLEM

The stability problem for modified potential flows over viscoelastic compliant layers (see Figure 1) is formulated here as a generalized matrix eigenvalue problem. We shall restrict our consideration to two-dimensional wave modes. Yeo [15] has shown that the most dominant surface-related instability modes, the type considered in this paper, are two-dimensional. The linear spanwise formation of the slow wave ridges in Gad-el-Hak *et al.* [1] also testifies to their two-dimensionality.

The velocity potential of an x_1-travelling wave perturbation in a uniform potential flow domain has the form:

$$\phi = A \cdot \exp(-\alpha x_2) \exp(\mathrm{i}\alpha x_1 - \mathrm{i}\omega t), \tag{1}$$

where A is a complex constant, and α and ω are the wavenumber and radian frequency of the wave respectively. The pressure perturbation acting on the compliant surface due to the flow may be derived from a direct application of Bernoulli's theorem to be

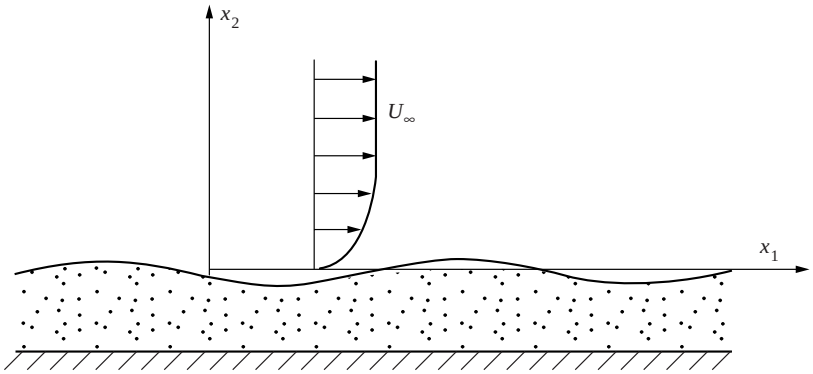

Figure 1. Fluid flow over a viscoelastic compliant layer.

$$p_s = \hat{p}_s \exp(\mathrm{i}\alpha x_1 - \mathrm{i}\omega t),$$

where $\hat{p}_s$ is the complex amplitude given by

$$p_s = -\mathrm{i}\alpha A(U_\infty - c). \tag{2}$$

$c = \omega/\alpha$ is the complex phase speed of the wave perturbation.

Uniform potential flow represents the limiting form of laminar and turbulent boundary layers as their thickness tends to zero. Duncan *et al.* [4] assumes the pressure fluctuations acting on the compliant wall in the presence of a boundary layer to be given by the pressure fluctuations (2) of the corresponding potential flow modified by a complex factor $K_p e^{\mathrm{i}\theta p}$:

$$\hat{p}_s = -K_p \exp(\mathrm{i}\theta_p)\mathrm{i}\alpha A(U_\infty - c). \tag{3}$$

The real coefficient K_p, which is generally <1, scales the magnitude of pressure fluctuation in a potential flow to the level encountered in the boundary layer. θ_p sets the phase angle of the pressure fluctuation relative to the vertical displacement of the compliant surface. It affects directly the transfer of energy from the flow to the wall. Flows with fluctuating pressure amplitude at the wall $\hat{p}_s$ prescribed by equation (3) are termed *modified potential flows* in this paper for ease of reference.

The parameters K_p and θ_p are, in general, functions of the wavenumber and frequency of the disturbance wave. Carpenter and Gajjar [16] presented an analytical approximation for pressure fluctuations in boundary-layer flows over bending plates. The pressure approximation may theoretically be used to estimate quantities such as the K_p and θ_p. Unfortunately, the approximation fails as the phase speed $c \to 0$, and is thus unsuitable for application to static divergence study. For applications to incompressible viscoelastic layers, the long-wave assumption ($\alpha \ll 1$) inherent in their theory may also become a restricting factor since such layers (unlike bending plates) may support short wavelength

instabilities because of their compliance at high wavenumbers. It is also unclear if the analytical approximation for pressure may be extended to account for turbulent fluctuations present in turbulent boundary layers.

For simplicity, the parameters K_p and θ_p are assumed to be constants in the present model of pressure fluctuations under a boundary layer. Duncan *et al.* [4] obtained suitable values of K_p and θ_p for turbulent boundary layers from the experimental data of Kendall [17]. For laminar boundary layers, corresponding values were obtained from the direct numerical simulation results of Balasubramanian and Orszag [18]. The values of K_p and θ_p employed by Duncan *et al.* will be adopted in this study. Duncan *et al.* have demonstrated that this relatively simple approach is adequate for eliciting the major behavioural trends and qualitative relationships when reasonable ranges or typical values are employed for the parameters.

The displacement of the corresponding two-dimensional wave in the compliant wall is given by

$$(\eta_1, \eta_2) = (\hat{\eta}_1, \hat{\eta}_2) \exp(\mathrm{i}\alpha x_1 - \mathrm{i}\omega t), \tag{4}$$

where $\hat{\eta}_1(x_2)$ and $\hat{\eta}_2(x_2)$ are amplitude functions which describe the variation of perturbation amplitude in the thickness direction of the compliant layer. For an homogeneous isotropic compliant layer (effects of body force neglected) the propagation of the wave is governed by the following viscoelastic analogue of Navier's equations (see reference [19]):

$$G(\hat{\eta}_1'' - \alpha^2 \hat{\eta}_1) - \left(K + \frac{G}{3}\right)(\alpha^2 \hat{\eta}_1 - \mathrm{i}\alpha \hat{\eta}_2') + \rho\omega^2 \hat{\eta}_1 = 0, \tag{5a}$$

$$G(\hat{\eta}_2'' - \alpha^2 \hat{\eta}_2) + \left(K + \frac{G}{3}\right)(\mathrm{i}\alpha \hat{\eta}_1' + \hat{\eta}_2'') + \rho\omega^2 \hat{\eta}_2 = 0. \tag{5b}$$

A prime denotes ordinary derivative in the x_2-direction. G and K are the shear and bulk moduli of the compliant material, respectively. Viscoelastic damping behaviour is modelled by assuming a Voigt solid for the compliant materials in shear:

$$G = G_r + \mathrm{i}G_i = \rho C_t^2 i - \mathrm{i}\omega d, \tag{6}$$

where ρ, C_t and d are respectively the material density, the elastic shear wave speed and the damping coefficient of the material. These and other physical quantities employed in the paper may be assumed to have been non-dimensionalized with respect to the following reference scales: U_∞, the free-stream velocity of the flow; the density of the flow; and the thickness of the compliant layer. The non-dimensional thickness of the compliant layers is therefore 1·0 throughout this paper. As the compliant coating materials tested by Gad-el-Hak *et al.* [1] and others have densities which are close to that of water, the test fluid, it shall henceforth also be assumed that the non-dimensional material density of the compliant layers is $\rho = 1{\cdot}0$.

Interaction between the flow and the compliant layer is governed by continuity conditions at their interface at $x_2 = 0$. The continuity of normal velocity yields

$$A = -\mathrm{i}(U_\infty - c)\hat{\eta}_2|_{x_2=0}, \tag{7}$$

The continuity of normal and shear stresses are given by:

$$2G\hat{\eta}_2' + \left(K + \frac{G}{3}\right)(\mathrm{i}\alpha\hat{\eta}_1 + \hat{\eta}_2') = -\hat{p}_s, \quad G(\hat{\eta}_1' + \mathrm{i}\alpha\hat{\eta}_2) = 0, \tag{8a, b}$$

where $\hat{p}_s$ denotes the complex amplitude of fluid pressure acting on the compliant surface, given by equation (3). Equation (8b) is a statement of the assumption that the flow exerts negligible shear stress on the compliant surface.

The compliant layer is assumed to be attached to a rigid base at $x_2 = -1$ (non-dimensionalized by the thickness of the compliant layer). This yields the following boundary conditions on the displacement functions:

$$\hat{\eta}_1|_{x_2=-1} = 0 \qquad \text{and} \qquad \hat{\eta}_2|_{x_2=-1} = 0. \tag{9a, b}$$

The wall equations (5a, b) and its four boundary conditions (8a, b) and (9a, b), with fluid pressure $\hat{p}_s$ prescribed by (3) and (7), form a homogeneous system of equations which constitutes the stability eigenvalue problem.

A Chebyshev collocation procedure is employed in the formulation of the stability eigenvalue problem as a generalized linear matrix eigenvalue problem for complex frequency ω. Yeo *et al.* [14] first carried this out for flow over viscoelastic compliant layers. The complex wall displacement function $\hat{\eta}_1(x_2)$ and $\hat{\eta}_2(x_2)$ are approximated by Chebyshev polynomial series of the Mth order:

$$\hat{\eta}_1(x_2) = \sum_{j=0}^{M} a_j T_j[\xi(x_2)], \tag{10a}$$

$$\hat{\eta}_2(x_2) = \sum_{j=0}^{M} b_j T_j[\xi(x_2)], \tag{10b}$$

where $\xi(x_2) = 1 + 2x_2$ is a transformation function which maps the wall domain $[-1, 0]$ onto the domain $[-1, 1]$ of the Chebyshev polynomials. M should be large enough to ensure adequate resolution of the vertical structure of the wave perturbation in the compliant layer. Typical values of M range from 20 to 40. The substitution of the Chebyshev representations (10a, b) into the governing equations (5a, b) and boundary conditions (8a, b) and (9a, b) produces a system of linear algebraic equations in the polynomial coefficients a_j and b_j. The complex frequency ω appears non-linearly (quadratic order) in the wall equations (5a, b) and boundary condition (8b). The problem is rendered linear in ω by introducing the auxiliary vectors $\omega\mathbf{a}$ and $\omega\mathbf{b}$ where $\mathbf{a} = (a_0, a_1, \ldots, a_M)$ and $\mathbf{b} = (b_0, b_1, \ldots, b_M)$ are vectors of the polynomial coefficients. The final assembled form of the matrix eigenvalue equation is

$$\left\{ \begin{bmatrix} \mathbf{A}_{11} & \mathbf{A}_{12} & \mathbf{A}_{13} & \mathbf{A}_{14} \\ \mathbf{A}_{21} & \mathbf{A}_{22} & \mathbf{A}_{23} & \mathbf{A}_{24} \\ \mathbf{0} & \mathbf{0} & \mathbf{I} & \mathbf{0} \\ \mathbf{0} & \mathbf{0} & \mathbf{0} & \mathbf{I} \end{bmatrix} - \omega \begin{bmatrix} \mathbf{B}_{11} & \mathbf{B}_{12} & \mathbf{B}_{13} & \mathbf{B}_{14} \\ \mathbf{B}_{21} & \mathbf{B}_{22} & \mathbf{B}_{23} & \mathbf{B}_{24} \\ \mathbf{I} & \mathbf{0} & \mathbf{0} & \mathbf{0} \\ \mathbf{0} & \mathbf{I} & \mathbf{0} & \mathbf{0} \end{bmatrix} \right\} \begin{Bmatrix} \mathbf{a} \\ \mathbf{b} \\ \omega\mathbf{a} \\ \omega\mathbf{b} \end{Bmatrix} = \{\mathbf{0}\}. \quad (11)$$

For a given set of wall properties and wavenumber α, all the temporal eigenvalues ω of equation (11) may be obtained by applying the standard QZ algorithm.

This formulation allows all the ω eigenvalues to be found without the need for any guess values. It has considerable advantage over traditional shooting methods, which generally require a guess value for the determination of each eigenvalue. Frequently, poor guess values lead to slow or even non-convergence of the shooting procedure. In applying shooting methods, an eigenvalue search procedure may have to be instituted to ensure that the important eigenvalues are not missed out due to poor choice of guess values.

The conventional procedure for finding absolute and convective instabilities, which is based on a direct interpretation of the theory by Briggs [12], requires the tracking of the α-eigenmodes (α-roots) in the complex α-plane as the imaginary part of frequency (ω_i) is varied. The task of following the α-roots and looking out for their intersections is a highly laborious one. A more efficient procedure devised by Kupfer *et al.* [20] to find the instabilities is employed in the present paper. The method is based on an examination of contours of constant α_i in the ω-plane. The formulation of the stability problem as a linear matrix eigenvalue problem in ω for prescribed values of α facilitates the construction of such contours. Absolute instabilities, which are formed from the coalescence of two or more α-roots in the α-plane, show up as *cusp points* in the α_i-contours in the ω-plane. The cusp is formed as a result of the period-doubling or -tripling characteristics of the local $\alpha \mapsto \omega$ map at points of eigenvalue- or root-intersection. However, not all cusp points in the ω-plane are admissible as absolute instability. The cusp point of an absolute instability must lie in the upper half of the ω-plane (i.e., $\omega_i > 0$). Furthermore, the manner of the associated root intersection in the α-plane must satisfy specific causality condition. In the ω-plane, the causal requirement may be verified by extending a vertical line upwards from the cusp point and determining the number of times this line intersects the $\alpha_i = 0$ contour. An odd number of intersections signifies a genuine absolute instability eigenstate.

Convective instabilities have real ω and complex α ($\alpha_i < 0$ for downstream growing modes and $\alpha_i > 0$ for upstream growing modes). These modes are thus distributed along the real axis of the ω-plane. Genuine convective instabilities must also satisfy the requirement of causality. The causality check procedure for absolute instability is also applicable to convective instability. The reader is referred to Bers [13] and Kupfer *et al.* [20] for details.

The greater ease of detecting mode coalescence aside, analysis in the ω-plane also confers other advantages. Every absolute and convective instability is contiguously linked to an unstable temporal branch. By focusing on events in the ω-plane, there is thus the additional benefit that only ω-branches which

exhibit temporal instability would need to be searched for the spatial-temporal modes. In most physical problems, there are usually only a small number of unstable temporal branches to reckon with (compared with the numerous α-roots that must be tracked for every unstable ω-branch). Also, many physical problems (including the present one) are more conveniently formulated as a linear matrix eigenvalue problem in ω than they are in α because of the higher polynomial degree of the latter. The matrix eigenvalue approach generally allows all the unstable ω-branches to be identified.

3. RESULTS AND DISCUSSION

Two main categories of flows are examined in this paper for the occurrence of absolute and convective instabilities: namely uniform potential flow, and modified potential flows representing turbulent and laminar boundary layers. We will focus more attention on the turbulent flow case since experimental data on it are more complete. In each case, the temporal instability of the flow was first studied, via the solution of equation (11) for real α, to locate the unstable branches. Mapping analyses were then carried out on the unstable temporal branches to identify the spatio-temporal instabilities and their type. It is pertinent to note that temporal instability is a necessary condition for the existence of both convective and absolute instabilities. The present study is expected to yield instabilities of the hydroelastic or surface-related category (associated with interaction of inertia, wall elasticity and energy transfer effects). The present simplified flow model may not capture the Tollmien–Schlichting class of instabilities, which requires explicit modelling of fluid viscosity.

3.1. UNIFORM POTENTIAL FLOW

Temporal study shows that uniform potential flow over viscoelastic compliant layers becomes unstable when the free-stream velocity U_∞ exceeds $1{\cdot}4142C_t$. This is in agreement with the numerical results of Duncan *et al.* [4]. In the range of U_∞ considered, up to $6C_t$, there appears to be only one unstable temporal branch. It is possible additional unstable temporal branches may appear at even higher speeds, but the branch considered here, with its relatively lower onset velocity, is the dominant temporal branch. The onset velocity of temporal instability at $U_\infty = 1{\cdot}4142C_t$ is unaffected by the level of material damping in the layer.

Figure 2(a) shows the mapping of the α_i-contours in the complex ω-plane for the case of a compliant layer with $U_\infty = 3C_t$ and material damping coefficient $d = 0{\cdot}05$. The $\alpha_i = 0$ contour marks out the temporal eigenmodes. It forms a loop which crosses over itself at the origin point $\omega = 0$. The loop itself is located in the upper half of the ω-plane ($\omega_i > 0$) and thus comprises unstable temporal modes. The $\alpha_i = 0$ loop encloses a cusp point I, which indicates a possible mode of absolute instability. Compliance with causality requirement may be verified by extending a straight line vertically upwards from the cusp point and ascertaining the number of times the line intersects the $\alpha_i = 0$ contour. It is readily seen that such a straight line would intersect the said contour only once. This confirms

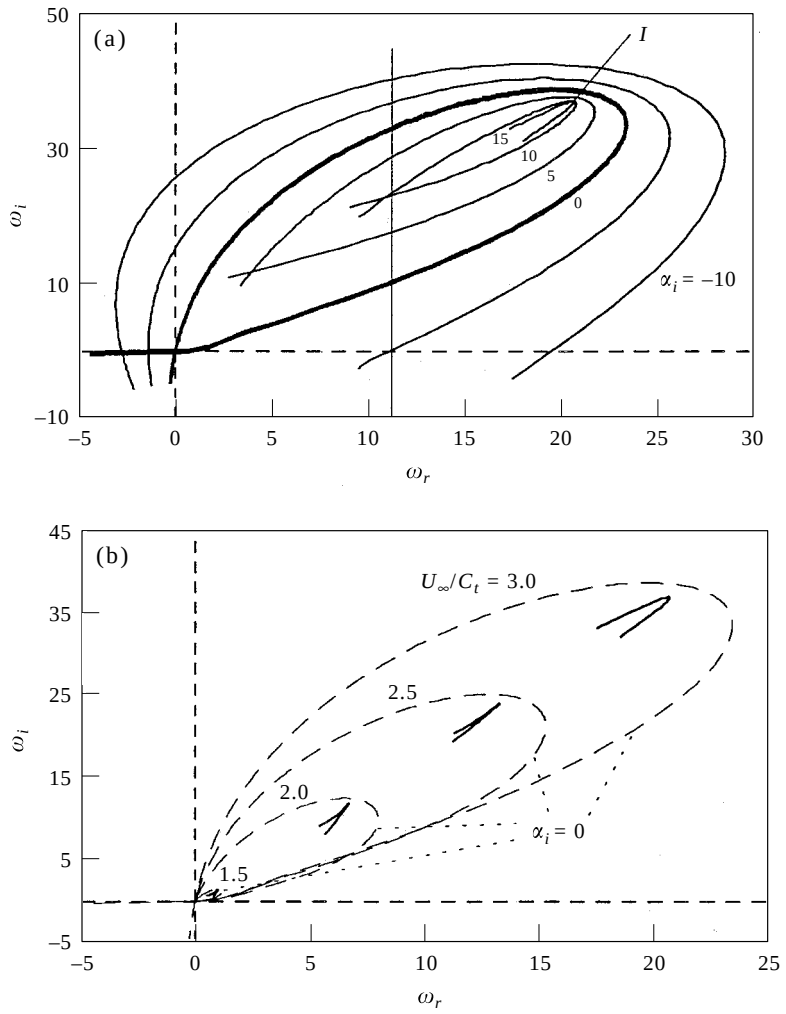

Figure 2. (a) The α_i-contours in the complex ω-plane for a potential flow at $U_\infty = 3{\cdot}0C_t$, $d = 0{\cdot}05$. The cusp point occurs at point *I*. (b) The effects of shear-wave speed C_t on the $\alpha_i = 0$ contour and cusp point. Increase in C_t causes the $\alpha_t = 0$ loop to shrink towards the origin $\omega = 0$.

that the cusp point indeed represents an absolute instability eigenstate, and that uniform potential flow over the compliant layer admits absolute instability.

The effects of shear-wave speed C_t (which governs the stiffness of the compliant layer) on the $\alpha_i = 0$ contour and the cusp point are depicted in Figure 2(b). Increase in C_t (or reduction in U_∞) causes the $\alpha_i = 0$ loop in the upper-half plane to tighten and shrink towards the origin $\omega = 0$. The shrinking of the loop takes place within the upper-half plane, with the cusp point being entrapped within the loop throughout. The loop eventually vanishes into the origin as U_∞/C_t is decreased to a value 1·4142, at which point the loop is itself transformed into the cusp that it encloses. $U_\infty/C_t = 1{\cdot}4142$ is also precisely the threshold value for the onset of temporal instability as noted earlier. This is no mere coincidence

of course, since the appearance of the loop (which occurs when U_∞/C_t becomes larger than 1·4142) in the upper-half plane ($\omega_i > 0$) also marks the onset of temporal instability. This shows that the absolute instability of uniform potential flow over viscoelastic compliant layers sets in at the point of the flow becoming temporally unstable.

One can usually ignore the occurrence of convective instability (if any) when there is absolute instability. This is because the latter is a more devastating form of instability. For completeness sake, however, we shall nevertheless attempt to characterize the occurrence of convective modes here. Convective instabilities in an open system may take the form of a downstream-growing ($\alpha_i < 0$) or an upstream-growing ($\alpha_i > 0$) sinusoidal wave mode of real frequency ($\omega_i = 0$). They are hence to be found on the real axis of the ω-plane. Figure 2(a) shows that the eigenmodes on the real-ω axis have $\alpha_i < 0$. These modes would give rise to downstream convective instability of the flow if they can be shown to satisfy the necessary causality condition. Causality is again verified by extending a straight line vertically upwards from the eigenmodes concerned and counting the number of times the drawn line intersects the $\alpha_i = 0$ contour. In Figure 2(a), such a line drawn from the real-ω axis may be seen to intersect the $\alpha_i = 0$ contour zero or two times. These are hence not true convective instability modes; and they have been termed *evanescent* modes* in the literature.

The above results indicate that uniform potential flow over viscoelastic layers (dissipative) admits only absolute instability. Absolute instability sets in as the flow becomes unstable according to normal-mode temporal theory. Since the onset of temporal instability in uniform potential flow is unaffected by the level of material damping in the wall, the onset flow velocity for absolute instability would remain constant at $U_\infty = 1{\cdot}4142C_i$ for all d. Similar studies of membrane and plate surfaces on damped elastic foundation also yield only absolute instability.†

3.2. MODIFIED POTENTIAL FLOW

The spatio-temporal stability disposition of modified potential flow representing turbulent and laminar boundary layers will now be examined. For turbulent layers, the parameters are assigned the value $K_p = 0{\cdot}25$ and $\theta_p = -10^\circ$ following Duncan *et al.* [4], who obtained these values from the experiments of Kendall [17]. These values are applicable for wavelength/displacement-thickness ratio λ/δ^* in the range of 14 to 20, which falls midway between the experimental ranges of Gad-el-Hak *et al.* [1] (about 3 to 8·5) and Hansen *et al.* [3] (about 20–40).

The α_i contours for turbulent boundary layer over a viscoelastic compliant layer wall with $C_t = 0{\cdot}333$ ($U_\infty = 3{\cdot}0C_t$) and $d = 0{\cdot}03$ are given in Figure 3(a). The $\alpha_i = 0$ contour differs significantly from the case of a uniform potential flow: it does not loop over itself in this part of the ω-plane, nor pass through the origin

* Conventional normal-mode spatial theory, which does not consider causation, is not able to distinguish between genuine convective instabilities and evanescent modes.

† Both absolute and convective waves modes were, however, found by Brazier-Smith and Scott [21] on unsupported elastic (non-dissipative) plate surfaces.

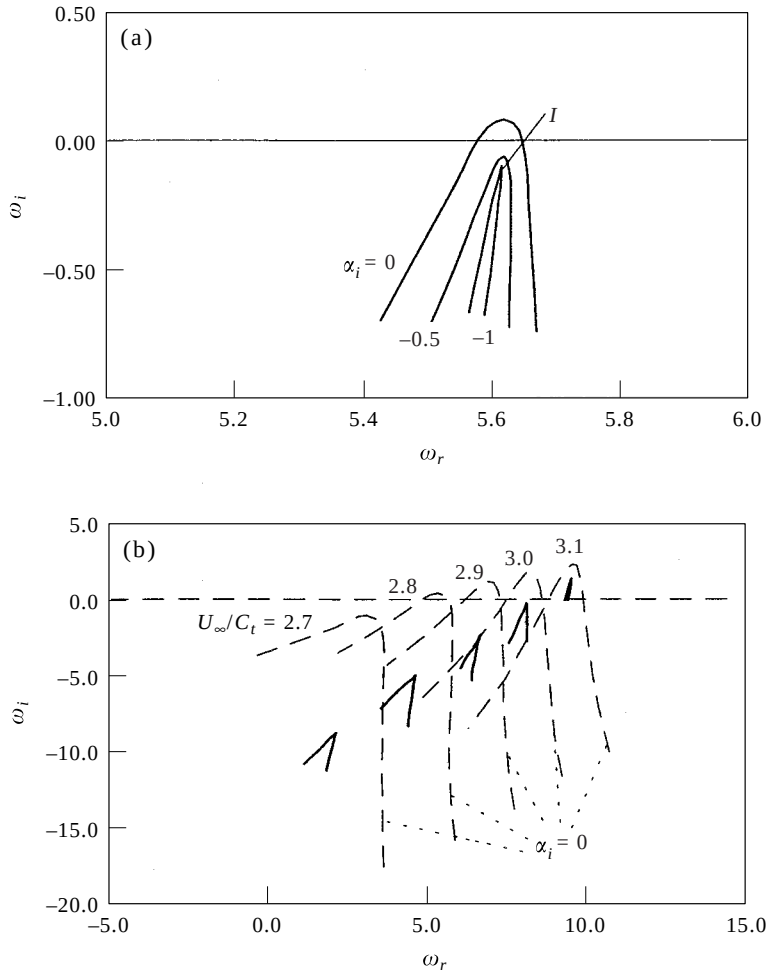

Figure 3 (a) The α_i-contours in the complex ω-plane for turbulent boundary-layer flow over a viscoelastic layer at $U_\infty = 3{\cdot}0C_t$, $d = 0{\cdot}03$. (b) The variation of the $\alpha_i = 0$ contour and cusp point with C_t for a turbulent boundary-layer flow at wall damping $d = 0{\cdot}02$. The onset velocities $U_\infty^{(conv)} = 2{\cdot}78C_t$ and $U_\infty^{(abs)} = 3{\cdot}02C_t$.

of the plane. The flow-wall combination is evidently unstable since part of the $\alpha_i = 0$ contour lies in the upper-half ω-plane. A cusp point is detected in the figure, but it does not constitute an absolute instability since $\omega_i < 0$ at the cusp point. Causal convective eigenstates are to be found, however, along the real-ω axis between the intercepts of the axis with the $\alpha_i = 0$ contour ($5{\cdot}57 < \omega_i < 5{\cdot}64$). These have $\alpha_i < 0$, which indicates that they are downstream growing real-frequency sinusoidal wave modes. They give rise to convective instability. The flow is hence *convectively* unstable.

Figure 3(b) depicts the variations of the $\alpha_i = 0$ contour and the cusp point with the shear-wave speed C_t of the viscoelastic layer. Reduction in C_t (or increase in U_∞/C_t) causes the $\alpha_i = 0$ contour and the cusp point to rise in the ω-plane, eventually resulting in the flow becoming convectively and then absolutely

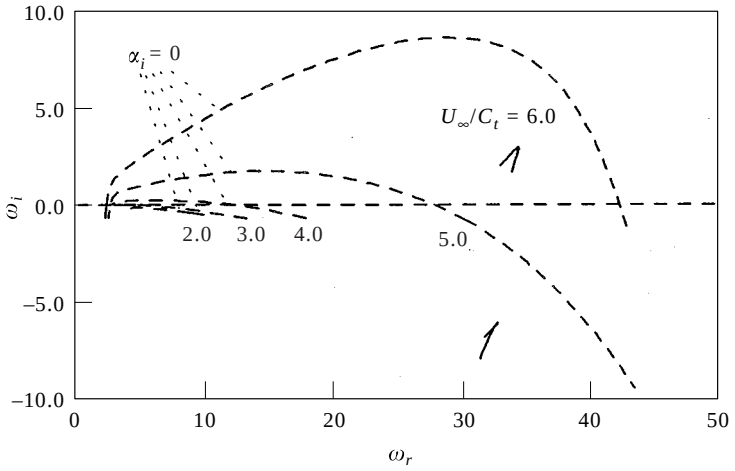

Figure 4. The variation of the $\alpha_i = 0$ contour and cusp point with C_t for a laminar boundary-layer flow at wall damping $d = 0{\cdot}01$. The onset velocities $U_\infty^{(conv)} = 2{\cdot}84C_t$ and $U_\infty^{(abs)} = 5{\cdot}83C_t$.

unstable as each (the $\alpha_i = 0$ contour and cusp point) crosses the real-ω axis in turn. Convective and absolute instabilities occur respectively at $C_t = 0{\cdot}36$ ($U_\infty = 2{\cdot}768C_t$) and $0{\cdot}33$ ($U_\infty = 3{\cdot}02C_t$). The geometrical relationship between the cusp point and the *over-arching* $\alpha_i = 0$ contour reveals that convective instability will always precede the absolute instability as the flow velocity U_∞ is increased. The flow continues to be convectively unstable in the presence of the absolute instability.

A broadly similar pattern of behaviour in the ω-plane is followed by laminar boundary layers for which the following values of $K_p = 0{\cdot}067$ and $\theta_p = -30°$ [4] have been used. Figure 4 depicts the $\alpha_i = 0$ contours for a range of U_∞/C_t from $2{\cdot}0$ ($C_t = 0{\cdot}5$) to $6{\cdot}0$ ($C_t = 0{\cdot}167$). Only cusp points at $U_\infty/C_t = 6{\cdot}0$ and $5{\cdot}0$ are shown, as the rest are beyond the range of the figure. Absolute instability occurs at an onset velocity of $U_\infty > 5{\cdot}83C_t$ ($C_t < 0{\cdot}171$), which is significantly higher than the $3{\cdot}02C_t$ for the turbulent boundary layer considered above. Another significant difference between the results for the laminar and turbulent cases lies in the broad sweep of the $\alpha_i = 0$ contours for the former compared to the rather peaky maximum of the latter (see Figure 3). The very peaky maximum of the $\alpha_i = 0$ contour suggests that incipient convective instability of the turbulent boundary layers will be very narrow-banded in α and ω. This seems to be in agreement with the highly regular sinusoidal form of the wave trains that Gad-el-Hak [2] had observed on nearly elastic layers, which signifies the presence of a fairly well-defined normal mode. On the other hand, for the laminar boundary layer (with its highly diffused maximum point), there is greater likelihood that the spectrum of unstable modes at the onset of convective instability will be broad-banded, so that no well-defined wave train may be discerned. The latter would make the visual detection of incipient convective modes more difficult.

The effects of material damping on the onset of absolute and convective instabilities for the turbulent boundary layers are shown in Figure 5. The onset

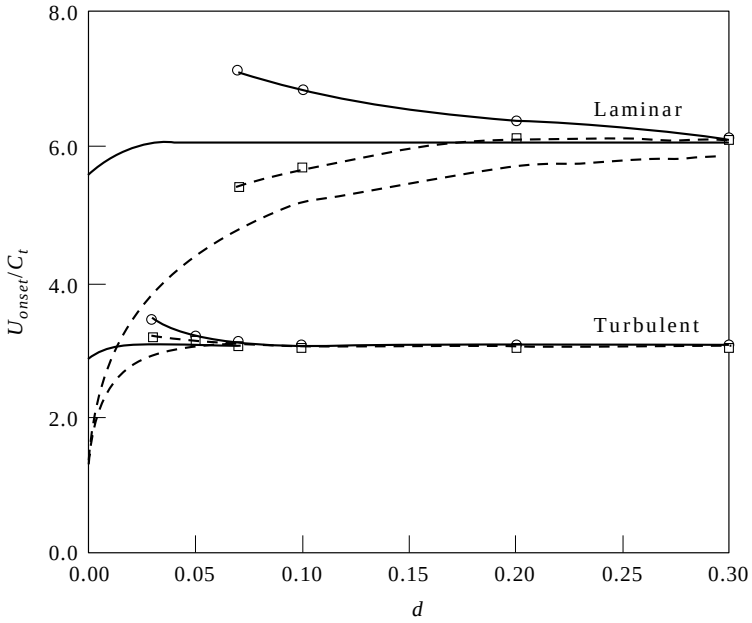

Figure 5. The effects of material damping on the onset of absolute (——) and convective (– – –) instabilities for laminar and turbulent boundary layers. The symbols ○ and □ denote results for the case of variable K_p and θ_p.

velocity of absolute instability, which is hereafter denoted by $U_\infty^{(abs)}$, remains relatively constant at about $3{\cdot}0C_t$, dipping slightly to $2{\cdot}86C_t$ as damping coefficient $d \to 0$. The computed absolute instability eigenstates have relatively small wavelengths and are thus, in a strict sense, valid only for fairly thick compliant layers. The temporal instabilities obtained by Duncan *et al.* [4] also have small wavelengths.* Gad-el-Hak *et al.* [1] found that the onset U_∞ of the slow waves varies with the thickness of the compliant layers. The onset U_∞ decreases from about $8C_t$ for a thin coating of 0·15 cm to $4{\cdot}5C_t$ for a thicker coating of 0·71 cm. The computed onset velocity of $3{\cdot}0C_t$ is therefore consistent with the observed trend for the slow waves.

The onset velocity for the convective instability (denoted by $U_\infty^{(conv)}$ for brevity) of the turbulent boundary layer starts at a value of $U_\infty = 0{\cdot}9553C_t$ for a nearly elastic layer ($d \to 0$). This is the Rayleigh surface-wave speed of the layer. Indeed as $d \to 0$, the $U_\infty^{(conv)}$ for both turbulent and laminar boundary layers do not depend on K_p and θ_p, but can be shown to tend to the same Rayleigh wave speed limit of the wall $c_R = 0{\cdot}9553C_t$ in accordance with the free-wave criterion in Yeo and Dowling [10]. The onset velocity $U_\infty^{(conv)}$ increases with d indicating the Class B character of the convective modes. The increase is fairly steep at first, but tapers off as $U_\infty^{(conv)}$ approaches the onset velocity of the absolute instability $U_\infty^{(abs)}$. The $U_\infty^{(abs)}$ acts as an upper bound to the $U_\infty^{(conv)}$,

* The present flow model lacks a well-defined flow lengthscale to pin down the unstable wavelength accurately. It has a tendency to pick high wavenumber instabilities because of the greater compliance of the compliant layer to those modes.

since $U_\infty^{(conv)} \leqslant U_\infty^{(abs)}$ as noted earlier. The $U_\infty^{(conv)}$ is thus forced to travel just below the $U_\infty^{(abs)}$ curve as d becomes large, with $U_\infty^{(conv)}$ tending ever closer asymptotically to $U_\infty^{(abs)}$ as d is further increased. Examination of the ω-plane reveals that the cusp-point eigenstate gradually approaches the maximum point of the $\alpha_i = 0$ contour as d becomes large. The traversing of the real-ω axis by the maximum point and the cusp point marks the onset of convective and absolute instabilities, respectively. Further numerical study suggests that the two points would converge in the limit of infinitely large d. Upon their convergence, the resultant eigenmode will be an absolute instability. The convective (and also temporal) instability of the flow would then become synonymous with its absolute instability; a situation similar to that for uniform potential flow considered earlier. Preliminary results from full modelling of the turbulent boundary layer (with eddy-viscosity modelling) lend support to what has been described above. The relative indifference of the onset velocity $U_\infty^{(abs)}$ for absolute instability (at larger d) suggests a Class C energy character for the instability. Lucey and Carpenter [23] also found similar Class C behaviour for SD-looking waves on a finite-length compliant panel in a potential flow. These are somewhat in contrast to the Class A finding of Yeo *et al.* based on viscous-flow modelling. However, given the simplicity of the flow model used here and in Lucey and Carpenter, the difference may not be surprising. We hope to resolve this point in our future work. It is also pertinent to note that as d becomes large, the phase speed of the convective instability mode slows down towards zero. Figure 6 shows the declining trend of the phase speed for convective instability modes in the turbulent boundary layer; c_r falls below $0{\cdot}05U_\infty$ for $d > 0{\cdot}1$. There is thus a close association between absolute instability and slowly moving convective modes.

The $U_\infty^{(abs)}$ and $U_\infty^{(conv)}$ curves for laminar boundary layers display many qualitative similarities with the results for turbulent layers (see Figure 5). The $U_\infty^{(abs)}$ also remains fairly constant and independent of the level of material damping. It hovers around $6{\cdot}0C_t$ over most of the damping range, and dips to $5{\cdot}63C_t$ as $d \to 0$. The $U_\infty^{(conv)}$ starts from $0{\cdot}9553C_t$ for a nearly elastic wall (as has already been mentioned), and rises in value towards $U_\infty^{(abs)}$ with increase in material damping. There is a noteworthy difference between the two sets of results though. Owing to the much larger value of the $U_\infty^{(abs)}$ for the laminar layer (which is about twice the value of the turbulent case) and the same starting value of $U_\infty^{(conv)}$ for both flows, a significant margin of difference continues to persist between the $U_\infty^{(abs)}$ and $U_\infty^{(conv)}$ even at a fairly large d. This means that the occurrence of absolute instability in laminar boundary layers is most likely preceded by the onset of strong convective instability. This agrees with what was also found by Yeo *et al.* [14].

At low levels of wall damping, the convective modes with their lower onset velocities are expected to be the dominant mode of instability. These modes travel at a fair speed and possess a sinusoidal form under incipient condition. There is little doubt the highly sinusoidal fast waves observed by Gad-el-Hak [2] over his nearly elastic compliant layers are waves of convective instability. Conventional normal-mode thinking has generally ascribed the appearance of

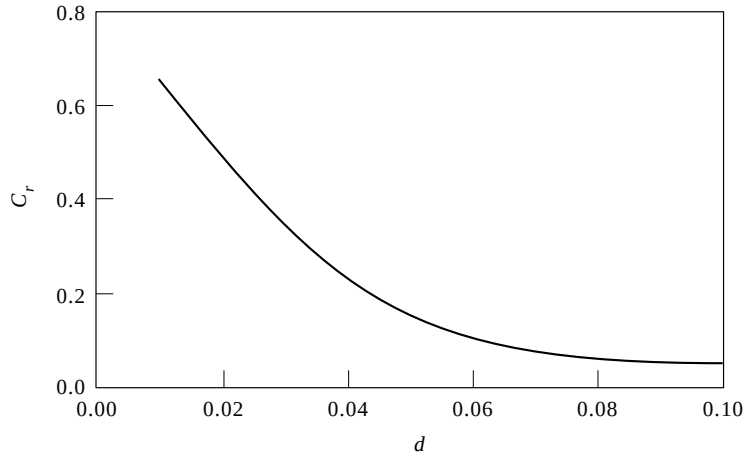

Figure 6. The effects of material damping on the phase speed of convective modes for a turbulent boundary-layer flow.

the slow wave (identified with Static Divergence) instability to the suppression of the fast waves (convective modes, travelling-wave flutter) by material damping (see references [10, 22], for example). Thus, high damping has been thought to have increased the onset flow velocity of the fast wave *above* the onset velocity of the SD mode (slow wave) so that the latter would become the dominant mode of instability. This has been the generally accepted explanation for the observation of slow waves in the experiments of Gad-el-Hak *et al.* [1]. As will be seen below, this simple interpretation of the experimental events may be further refined, and new insights gained, with the benefit of a spatio-temporal analysis.

Firstly, the onset velocity for the fast wave (convective mode) $U_\infty^{(conv)}$ can never increase above the onset velocity of the slow wave if the latter is associated with an absolute instability of the flow. This should remain true even if K_p and θ_p are not constant but functions of α and ω because the inequality $U_\infty^{(conv)} \leqslant U_\infty^{(abs)}$ is merely a fundamental consequence of the fact that the convective (fast) modes and the absolute instability mode are derived from the same temporal branch of instability. Secondly, the spatio-temporal results show that increase in damping merely causes the marginal fast-wave (convective) eigenmode and the slow-wave (absolute instability) eigenmode to converge. For turbulent boundary layers on a highly damped compliant wall, the close identity (proximity) of the two eigenmodes indicates that it would be very difficult to distinguish between them, especially in experiments given practical limitations on accuracy of control and measurements. In such a situation, absolute instability is likely to follow closely on the heel of any convective instability. It will quickly assert itself over the latter so that convective instability will be at best a fleeting phenomenon. It is pertinent at this juncture to recall an observation of Gad-el-Hak *et al.* [1] concerning the initial development of the slow waves. They noticed that the appearance of the large-amplitude slow waves is always preceded by a highly transitory small-amplitude wave train. It is entirely plausible the highly transient incipient wave train (which they could not record on film) actually represents the

initial onset of a convective mode. In the course of increasing the flow velocity U_∞ to initiate instability, the absolute instability mode with its marginally larger onset velocity might have been triggered at the same time, and it grew quickly to overwhelm any token of the weaker instability. Other indications supporting the view that the slow waves are produced by absolute instability include the temporal-like growth of the incipient slow waves. Gad-el-Hak *et al.* had also noted that the slow waves have *highly asymmetric waveform with sharp peaks and shallow troughs in between*. Absolute instabilities, which are derived from causal mode coalescence, are likely to have a non-sinusoidal appearance because their waveform contains contributions from a continuous spectrum. Non-linear effects are clearly also important in the development and equilibration of the final observed slow waves given their large amplitude; so not all features of the observed slow waves may be explained on the basis of the present linear study.

The present spatio-temporal results provide strong evidence that the observed slow (SD) waves on highly damped compliant walls are indeed manifestations of absolute instability. This may also be the reason why SD waves are commonly observed in both experiments and in the nature (the wrinkling waves on dolphins and humans in rapid swimming [24]) since these surfaces do possess significant levels of material damping. A wall with slightly lower damping might then show up the two stages of instability more clearly. Yet for a wall with very low damping (nearly elastic), it would be difficult to distinguish between the two instabilities since the flow and wall would be dominated by strong convective modes before the appearance of any SD mode.

It is less easy, however, to be definite about the cause for the absence of the SD or slow waves under conditions of laminar flow in Gad-el-Hak *et al.* [1]. It is possible the absence could be due to the disturbance-free environment of the towing tank under laminar flow conditions as Duncan *et al.* [4] had suggested. Other plausible explanations are suggested by the above laminar spatio-temporal results, which show that convective instability sets in at considerably lower onset velocities than absolute instability. The first is that the flow or towing speeds were simply not high enough for the tested surfaces, which for practical reasons could not be made with stiffnesses below a certain limit. The second is that strong convective instability could have prevailed over the flow before the onset velocity for absolute instability was reached, and had wrought changes to the flow that subsequently precluded the occurrence of absolute instability. A very high level of material damping would be required for slow (SD) waves to occur under a laminar boundary layer.

For plane channel-flow between compliant plates, Davis and Carpenter [25] have shown that SD type instabilities are prevented if the properties of the wall are such as to favour interactions between the most unstable (least-damped) TS modes of the flow and the lowest free wave speed of the plates. It is unclear if a similar condition also holds for viscoelastic layers. It is possible this condition may be related to a situation in which convective instability is the dominant mode and conditions (such as the onset velocity) admitting an absolutely unstable SD mode have not been reached.

Constant but representative values of K_p and θ_p have so far been employed in the above study for simplicity. However, many of the important qualitative features of stability behaviour discussed above are expected to remain valid if K_p and θ_p are allowed to vary. To be assured that the observed trends are not unduly affected by variation in the parameters, available data in Kendall [17] were used to model the variation of K_p and θ_p as functions of phase speed c_r/U_∞ (there is insufficient data in Kendall to model the effect of α). Variable K_p and θ_p are obtained by linearly interpolating their values between c_r/U_∞ of 0·0 and 0·25 (maximum available). The onset velocities for absolute and convective instabilities based on the above variation of K_p and θ_p are marked by circles and squares respectively in Figure 5. No results are shown for d less than about 0·03 because the c_r/U_∞ involved is outside the interpolation range. The variable K_p and θ_p results show slightly higher onset velocities towards lower damping (in agreement with the prediction of our preliminary eddy-viscosity turbulent-flow model). But more crucially, the qualitative feature of onset-velocity convergence with increasing material damping remains essentially the same as the constant parameter case, as expected.

For the laminar case, Orr–Sommerfeld calculation based on Yeo *et al.* [14] was first carried out to determine if the values of $K_p = 0{\cdot}067$ and $\theta_p = -30{\cdot}4^\circ$ used above were reasonable. These values were obtained by Duncan *et al.* from direct numerical simulation of flow over stationary ($c = 0$) finite waves of wavelength $\lambda/\delta^* = 12$. For Reynolds numbers of 1500 and 2000 (which are in the high flow speed range encountered in Gad-el-Hak *et al.*'s experiments, assuming the laminar boundary layer starts from the leading edge of the plate) and wavelength $\lambda/\delta^* \approx 12$ (mid-range of experimental results; see Duncan *et al.*), values of $K_p \approx 0{\cdot}067$, $\theta_p \approx -27{\cdot}2^\circ$ and $K_p \approx 0{\cdot}06$, $\theta_p \approx -27{\cdot}5^\circ$ were obtained, respectively, which are close to the adopted values. The variations of K_p and θ_p for values of c up to about 0·2 (low phase-speed regime) were also computed. The variations of K_p and θ_p with c are used to recompute the onset velocities as a function of material damping coefficient d. This is also depicted in Figure 5. Similar to the turbulent case, onset velocity for absolute instability rises as material damping is reduced, which is indicative of Class A energy behaviour. At the same time, the onset velocity for the convective modes decreases resulting in a rapid divergence of the two onset velocities towards lower d. There is thus a large onset velocity difference even at high values of d, similar to what has been observed for the constant K_p and θ_p case.

4. CONCLUSIONS

The spatio-temporal stability of uniform potential flow and modified potential flows, representing turbulent and laminar boundary layers, over viscoelastic compliant layers has been investigated qualitatively. The spatio-temporal approach offers insights into the stability behaviour of open systems that could not be gained from a purely temporal or spatial interpretation of instability.

The study reveals that the instability of potential flow over viscoelastic compliant walls is always absolute, with an onset flow velocity of $1{\cdot}4142C_t$ which

is independent of the level of wall damping. Turbulent and laminar boundary layers admit both convective (travelling type) and absolute (stationary type) instabilities. Convective instability has a lower onset velocity than absolute instability; $U_\infty^{(conv)} \leqslant U_\infty^{(abs)}$. Convective instability dominates in flow over compliant layers with low levels of material damping. Thus, the highly sinusoidal small-amplitude fast waves observed by Gad-el-Hak [2] on his nearly elastic layers are waves of convective instability. Increase in material damping causes $U_\infty^{(conv)}$ to rise progressively and asymptotically towards $U_\infty^{(abs)}$. The difference in the onset velocities for the two instabilities $(U_\infty^{(abs)} - U_\infty^{(conv)})$ is vanishingly small for turbulent boundary layers when damping becomes large. This is due to the relatively low value of the $U_\infty^{(abs)}$. Laminar boundary layers, on the other hand, have much larger $U_\infty^{(abs)}$, so that a significant difference in onset velocities $(U_\infty^{(abs)} - U_\infty^{(conv)})$ persists even to fairly high levels of damping. Convective instability may thus be expected to dominate in laminar boundary layers except at very high wall damping levels. Our results also show that the absolute instability and its associated convective instability eigenstates converge to each other in the limit of a very highly damped compliant wall. The limiting convective modes have phase speed tending to zero. This association indicates that the occurrence of absolute instability and zero-phase-speed wave on highly damped viscoelastic layers, as a cause for the observed slow waves under turbulent boundary layers, are closely related phenomena. It also suggests that, as a practical measure, the occurrence of absolute instability may be conveniently determined via the simpler temporal theory, where one would look for marginally unstable modes with small phase speed.

For a turbulent boundary layer over a significantly damped compliant layer, it may not be possible to distinguish experimentally between the two instabilities because of the very small onset velocity difference. Indeed, absolute instability is expected to dominate in such flows. The viscoelastic compliant walls of Gad-el-Hak *et al.* [1] possess significantly high levels of material damping. The present study provides convincing evidence that the observed large-amplitude slow waves are manifestations of absolute instability of the flow and wall.

REFERENCES

1. M. Gad-el-hak, R. F. Blackwelder and J. J. Riley 1984 *Journal of Fluid Mechanics* **140**, 257–280. On the interaction of compliant coatings with boundary-layer flow.
2. M. Gad-el-hak 1986 *Transactions of ASME, Series E: Journal of Applied Mechanics* **53**, 206–212. The response of elastic and viscoelastic surfaces to a turbulent boundary layer.
3. R. J. Hansen, D. L. Hunston, C. C. Ni and M. M. Reischman 1980 *Journal of Sound and Vibration* **68**, 317–334. An experimental study of flow-generated waves on a flexible surface.
4. J. H. Duncan, A. M. Waxman and M. P. Tulin 1985 *Journal of Fluid Mechanics* **158**, 177–197. The dynamics of waves at the interface between a viscoelastic coating and a fluid flow.

5. A. Evrensel and A. Kalnins 1988 *Transactions of ASME, Series E: Journal of Applied Mechanics* **55**, 660–666. Response of a compliant slab to viscous incompressible fluid flow.
6. P. W. Carpenter and A. D. Garrad 1985 *Journal of Fluid Mechanics* **155**, 465–510. The hydrodynamic stability of flow over Kramer-type compliant surfaces. Part I. Tollmien-Schlichting instabilities.
7. K. S. Yeo 1988 *Journal of Fluid Mechanics* **196**, 359–408. The stability of boundary-layer flow over single- and multi-layer viscoelastic walls.
8. T. B. Benjamin 1960 *Journal of Fluid Mechanics* **9**, 513–532. Effects of a flexible boundary on hydrodynamic stability.
9. M. T. Landahl 1962 *Journal of Fluid Mechanics* **13**, 609–632. On the stability of a laminar incompressible boundary layer over a flexible surface.
10. K. S. Yeo and A. P. Dowling 1987 *Journal of Fluid Mechanics* **183**, 265–292. The stability of inviscid flows over passive compliant walls.
11. T. B. Benjamin 1963 *Journal of Fluid Mechanics* **16**, 436–450. The threefold classification of unstable disturbances in flexible surfaces bounding inviscid flows.
12. R. J. Briggs 1964 *Electron-Stream Interaction with Plasmas*. Monograph No. 29. Cambridge, MA: MIT Press.
13. A. Bers 1983 *Handbook of Plasma Physics*. Amsterdam: North-Holland. See Chapter 3.
14. K. S. Yeo, B. C. Khoo and H. Z. Zhao 1996 *Theoretical and Computational Fluid Dynamics* **8**, 237–252. The absolute instability of boundary-layer flow over viscoelastic walls.
15. K. S. Yeo 1992 *Journal of Fluid Mechanics* **238**, 537–577. The three-dimensional stability of boundary-layer flow over compliant walls.
16. P. W. Carpenter and J. S. B. Gajjar 1990 *Theoretical and Computational Fluid Dynamics* **1**, 349–378. A general theory for two- and three-dimensional wall-mode instabilities in boundary layers over isotropic and anisotropic compliant walls.
17. J. M. Kendall 1970 *Journal of Fluid Mechanics* **14**, 259–281. The turbulent boundary over a wall with progressive waves.
18. R. Balasubramanian and S. A. Orsag 1983 *NASA Contract Rep*. 3669. Numerical studies of laminar and turbulent drag reduction.
19. D. R. Bland 1960 *Linear Viscoelasticity*. Oxford: Pergamon.
20. K. Kupfer, A. Bers and A. K. Ram 1987 *Physics of Fluids* **30**, 3075–3082. The cusp map in the complex-frequency plane for absolute instabilities.
21. P. R. Brazier-smith and J. F. Scott 1984 *Wave Motion* **6**, 547–560. Stability of fluid flow in the presence of a compliant surface.
22. P. W. Carpenter 1990 *Progress in Astronautics and Aeronautics* **123**, 79–113. Status of transition delay using compliant walls.
23. A. D. Lucey and P. W. Carpenter 1992 *Journal of Fluid Mechanics* **234**, 121–146. A numerical simulation of the interaction of a compliant wall and inviscid flow.
24. F. S. Essapian 1955 *Brevioria Museum of Comparative Zoology* **43**, 1–4. Speed-induced skin folds in the bottle-nosed porpoise, Tursiops truncatus.
25. C. Davis and P. W. Carpenter 1997 *Journal of Fluid Mechanics* **352**, 205–243. Instabilities in a plane channel flow between compliant walls.